ORIGINAL PAPER

# Co$_{core}$–Pt$_{shell}$ nanoparticles as cathode catalyst for PEM fuel cells

**Huimin Wu · David Wexler · Guoxiu Wang · Huakun Liu**

**Abstract** Nanoscale Co$_{core}$–Pt$_{shell}$ particles were successfully synthesized based on a successive reduction strategy. The as-prepared core–shell nanoparticles were characterized by X-ray diffraction, energy-dispersive X-ray spectroscopy, transmission electron microscope, and electrochemical methods. It was found that the catalytic reactivity of Co$_{core}$–Pt$_{shell}$/C catalysts toward oxygen reduction was enhanced. It is believed that the prepared Co$_{core}$–Pt$_{shell}$/C nanoparticles could be promising for cathode catalysis in proton exchange membrane fuel cells with much reduced Pt content, but significantly increased catalytic activity.

**Keywords** Core–shell · Proton exchange membrane fuel cells · Oxygen reduction · Cathode catalyst

## Introduction

Platinum is the most effective catalyst to facilitate both hydrogen oxidation and oxygen reduction in a proton exchange membrane (PEM) fuel cell [1–3], but several critical issues still need to be addressed before such cells can be commercialized for automotive application. For example, the oxygen reduction reaction (ORR) is kinetically limited at the cathode [4–7], while Pt-based catalysts lead to high costs.

During the last decade, there has been a surge in research on nanocrystals with core–shell architectures, owing to their superior catalytic [8–12], optical [13–15], magnetic [16–18], and electrical [19] properties. Among the core–shell nanoparticles in various combinations, those made of an inexpensive metal core and a noble metal shell have received particular interest because of the functional and economic advantages that they can provide [8–13, 20–22]. Arranging noble metals as thin shells on non-noble metal cores not only greatly reduces noble metal use but could also significantly enhance their catalytic properties via the underlying interface between the core and shell metals due to the bimetallic mechanism [23].

It has been shown that Pt–Co alloy could significantly improve the catalytic activity toward oxygen reduction [24–28] in fuel cells. Therefore, Co$_{core}$–Pt$_{shell}$ nanoparticles are expected to be highly functional materials for catalytic applications [29, 30]. Our objective in this study has been to synthesize such core–shell nanoparticles. The core–shell structure is realized via a successive reduction strategy and by carefully choosing an appropriate reducing agent [31]. The formation of the core–shell structure has been elucidated by various techniques, including transmission electron microscopy (TEM) and electrochemical techniques. Although the Co$_{core}$–Pt$_{shell}$ particles have a much reduced content of Pt, they exhibit significantly enhanced catalytic activity toward oxygen reduction as compared to pure Pt catalyst, showing their great promise in solving the problem of the high demand for precious platinum metal in the cathodes of state-of-the-art PEM fuel cells [32].

H. Wu (✉)
College of Chemistry & Chemical Engineering, Hubei University,
Wuhan 430062, People's Republic of China
e-mail: whm267@gmail.com

H. Wu · D. Wexler · G. Wang · H. Liu
Institute for Superconducting & Electronic Materials,
School of Mechanical, Materials and Mechatronics Engineering,
University of Wollongong,
Wollongong, NSW 2522, Australia

## Experimental

### Preparation of $Co_{core}$–$Pt_{shell}$ catalyst nanoparticles

*Synthesized step 1* The Co seed was prepared first. Briefly, poly(vinylpyrrolidone) (PVP; 78.8 mg, $M_W$=55,000, Aldrich) and $CoCl_2·6H_2O$ (103.8 mg, Aldrich, 99.9%) were dissolved in 30 mL of deionized water in a three-necked flask (equipped with a reflux condenser and electric stirrer), stirred, and purged in Ar for 30 min. Keeping the saturation Ar atmosphere, a freshly prepared strong reduction solution of $NaBH_4$ (6 mg in 30 mL 0.1 mol $L^{-1}$ NaOH solution) was then added dropwise into the above solution under stirring at room temperature for 30 min to quickly form the Co microcrystal cores. The solution was then heated to refluence, and 28 mL of a weak reduction agent, hydrazine hydrate (Aldrich) solution, was added dropwise with stirring. The mixture was reacted for 2 h, and the redundant hydrazine hydrate was completely washed away with water.

*Synthesized in step 2* Pt was then deposited onto the Co using the following method. $H_2PtCl_6·6H_2O$ (75.3 mg, Aldrich, 99.9%), oleylamine (2.0 mL, Sigma-Aldrich), and $NH_2OHHCl$ (50.49 mg, Sigma-Aldrich) were mixed with 60 mL water under vigorous stirring and heated at 60 °C for 3 h. This solution was then added to the Co seed solution, and the temperature was held constant at 60 °C for 2 h. After 2 h, the solution was cooled to room temperature and then filtered and washed with copious water. The final product was then dried at 60 °C under vacuum conditions overnight.

In order to obtain pure Co nanoparticles with a narrow size distribution, a "two-step" reduction method was employed with $NaBH_4$-NaOH as the nucleating agent and hydrazine hydrate as the reduction agent in our experiments, respectively. In the first step, $NaBH_4$-NaOH, a strong reduction agent, was used to quickly reduce part of the $Co^{2+}$ to form the Co microcrystal cores. PVP ($M_W$= 55,000) was used as a stabilizer to control particle sizes. In the second step, hydrazine hydrate, a weak reduction agent, was used to control the reduction speed of $Co^{2+}$ to achieve reduction of most of the cobalt ions and cause them to grow onto the Co microcrystal seed cores formed in the first step. With this "two-step" reduction method, it is easy to prepare pure Co nanoparticles [33].

To deposit platinum on the surface of the Co, $NH_2OHHCl$ was carefully chosen as the reducing agent because it is well-known that in a slightly acid environment, $NH_2OHHCl$ only acts as a growth agent without forming new nuclei [34, 35]. Oleylamine was chosen as the capping agent. During the heating pretreatment, where the $H_2PtCl_6·6H_2O$ solution, the oleylamine, and the $NH_2OHHCl$ solution were mixed, neither color change nor precipitation was observed until the addition of the Co seeds. This strongly suggests that $NH_2OHHCl$ only acts as a growth agent in the presence of preformed nuclei.

To prepare $Co_{core}$–$Pt_{shell}$/C particles, an appropriate amount of XC-72 carbon (Cabot Corp., Vulcan XC-72, purified and oxidized by following a procedure reported in [36]) was added to the $Co_{core}$–$Pt_{shell}$ particle solution according to the weight ratio of Co–Pt/C=20:80, and the mixture was stirred overnight. As a comparison, the electrochemical performance of the commercial Pt/C catalyst from BASF (20% Pt supported on Vulcan XC-72 carbon, BASF Chemical) was also examined.

### Measurements

The phase identity of the Pt/C (BASF) was characterized by X-ray diffraction (XRD), using a GBC MMA X-ray diffractometer with Cu Kα radiation. And we used theta–2theta arrangement in grazing incidence diffraction mode. XRD specimens were prepared by milling catalyst powder for a moment and putting on the glass using ethanol as dispersing and binding agent.

The morphology of the catalyst was observed by TEM, using a JEOL JEM 2011 TEM facility, with an energy-dispersive spectrometer. TEM specimens were prepared by making a suspension of catalyst powder in ethanol and depositing a drop of the suspension on a standard carbon-covered copper grid.

Electrochemical measurements were performed with a three-electrode configuration. Electrode ink was prepared by adding the catalyst powders to a 5-wt.% Nafion® solution (DuPont™) according to the ratio of 5 mg to 1 mL. The ink was subsequently treated ultrasonically for at least 1 h until the ink became attached to the bottle wall without macroscopic granules. The working electrodes were made by casting the ink as a thin film onto a glassy carbon rotating disk electrode (geometrical area= 0.196 cm²) with the Nafion acting as the binding agent. Then the electrode was heated for a moment to evaporate the agent. The counter electrode was a Pt wire (diameter is 1 mm), and the reference electrode was an Ag/AgCl/$KNO_3$ (10%) electrode. So, all potentials are measured with respect to the Ag/AgCl/$KNO_3$ (10%). The electrolyte solution was 0.1 mol/L $HClO_4$. All measurements were performed at room temperature (25 °C).

## Results and Discussion

Figure 1 shows the X-ray diffraction pattern of the Co nanoparticles (synthesized in step 1) and the $Co_{core}$–$Pt_{shell}$
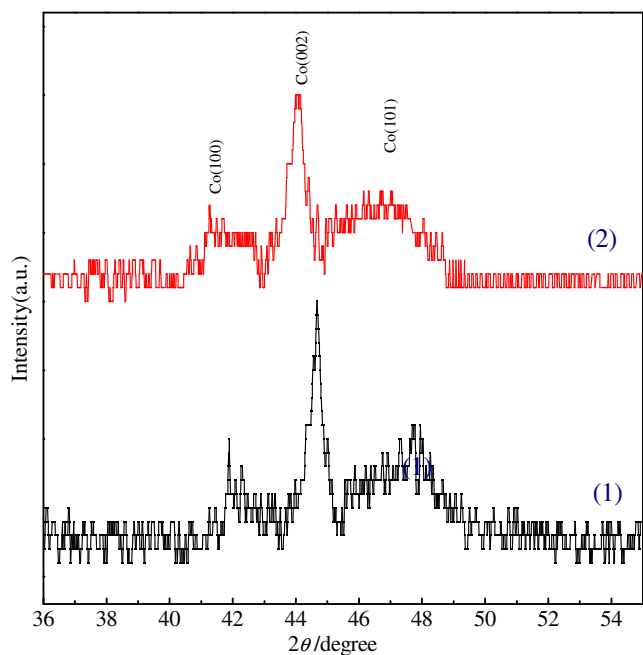
**Fig. 1** X-ray diffraction patterns of *1* Co nanoparticles (synthesized in step 1) and *2* Co$_{core}$–Pt$_{shell}$ nanoparticles (synthesized in step 2)

nanoparticles (synthesized in step 2). Only diffraction peaks of Co phase appeared in the XRD pattern. This could be because the outer Pt layer is too thin to be visible to X-ray diffraction. All diffraction lines can be indexed to the hexagonal close-packed (hcp) Co phase with the space group: P63-mmc, 194. No characteristic diffraction peaks of cobalt oxides were detected, indicating that the oxidation of Co can be effectively prevented by flowing argon gas during the reduction process. The value of the mean crystallite size of the Co$_{core}$–Pt$_{shell}$ catalysts is 3.25 nm, as determined quantitatively from XRD analysis.

Figure 2 is a high-resolution TEM (HRTEM) image of a large cluster of Co$_{core}$–Pt$_{shell}$ catalyst particles. We also performed quantitative energy-dispersive X-ray analysis on the sample. The atomic ratio of Pt/Co was determined to be 25.2:74.8, and this is consistent with the theoretical stoichiometric proportion of 1:3. The HRTEM image in Fig. 2 shows that the Co$_{core}$–Pt$_{shell}$ catalyst has a particle size in the range of 3 to 4 nm, which is consistent with the results deduced from XRD. Since the Pt shell is very thin, it is impossible to resolve the core–shell structure in this image. As showed in Fig. 2b, the lattice planes with a interlayer distance of 0.22 nm in the core can be indexed to (002) crystal planes of Co. The outer layer of the nanoparticles shows different contrast, which is the interface between the Co core and the surrounding. The whole area electron diffraction pattern is shown as the inset in Fig. 2c. The major diffraction rings can be indexed to be the hcp cobalt phase. As labeled on the SAED pattern, 1 weak diffraction ring can be identified as Pt(111), which confirms the co-existence of Co and Pt phase.

Electrochemical behaviors of materials are very sensitive to their surface composition and structures [32].

**Fig. 2 a** HRTEM image of Co$_{core}$–Pt$_{shell}$ catalyst; **b** enlargement of indicated area showing lattice spacing; **c** TEM image of Co$_{core}$–Pt$_{shell}$ catalyst, with the *inset* showing the whole area electron diffraction pattern
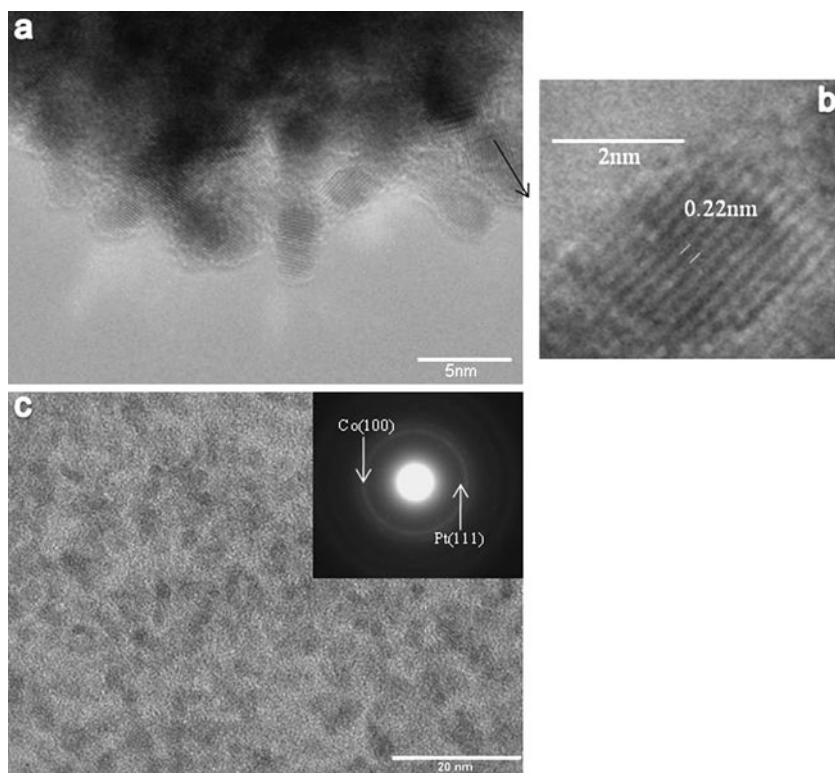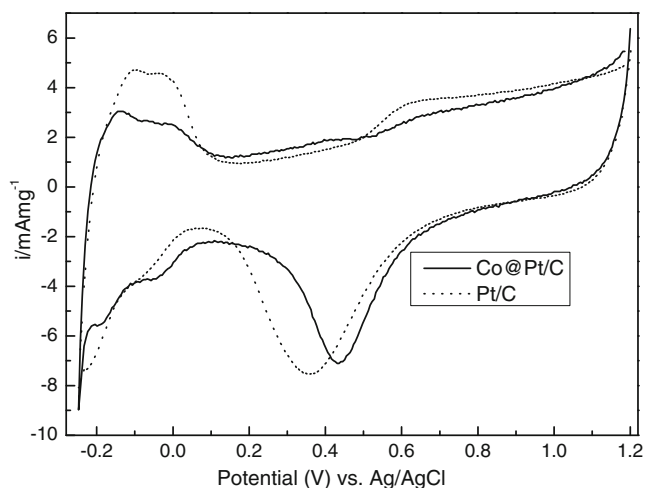
Fig. 3 Cyclic voltammograms of $Co_{core}$–$Pt_{shell}$/C and Pt/C catalysts in argon-saturated 0.1-mol/L $HClO_4$ electrolyte. Scanning rate, 50 mV/s



Fig. 4 Cathodic potential sweep curves for $a$ Pt/C and $b$ $Co_{core}$–$Pt_{shell}$/C in 0.1 M $HClO_4$ solution saturated with oxygen using a rotating disk electrode at 1,600 rpm and a scan rate of 10 mV/s

Solid evidence for the Pt coating comes from cyclic voltammetry (CV), as it can be regarded as a surface sensitive technique that only detects the electrochemical properties of surface atoms rather than bulk atoms. Figure 3 shows cyclic voltammograms for the particles prepared in this work and for the BASF Pt/C particles in argon-saturated 0.1 mol/L $HClO_4$ solution at a sweep rate of 50 mV/s.

The CV curves in Fig. 3 exhibit two distinctive potential regions associated with $H_{upd}$ adsorption/desorption ($H^+$ + $e \rightleftharpoons H_{upd}$) processed between $-0.25$ V$<E<0$ V and the formation of a $OH_{ad}$ layer ($2H_2O \rightleftharpoons OH_{ad} + H_3O^+ + e$) in the cathodic direction, where $H_{upd}$ and $OH_{ad}$ refer to the underpotentially deposited hydrogen and the adsorbed hydroxyl species, respectively. Furthermore, the particles exhibited well-defined current peaks associated with hydrogen adsorption–desorption processes on a Pt surface, implying a Pt nature of the particle surface. A current peak associated with the reduction of platinum oxide in the region of 0.35–0.65 V is also well-defined, and the onset current peak in the CV curve obtained from the $Co_{core}$–$Pt_{shell}$ particles is shifted by more than 50 mV toward positive potential as compared to that of the pure Pt particles. This implies that desorption of the hydroxyl species (e.g., OH) from the surface of a $Co_{core}$–$Pt_{shell}$ particle is easier than from the surface of a pure Pt particle. The major decline that generally occurs in a fuel cell's efficiency has been partly attributed to the inhibition of $O_2$

reduction caused by OH adsorption on Pt in the potential region of 0.75–1 V [5, 37]. Therefore, the weak adsorption of the hydroxyl species would increase the surface active sites for ORR [28, 38, 39] and thus the fuel cell's efficiency. By measuring the charges collected in the $H_{upd}$ adsorption/desorption region after double-layer correction (integrating the region of $H_{upd}$ adsorption/desorption and divided by the scan rate) and assuming a value of 210 μC/cm² for the adsorption of a hydrogen monolayer [40], the specific



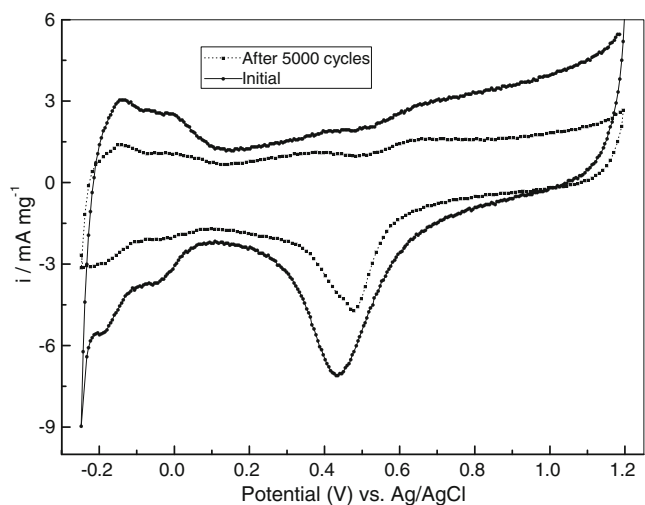Fig. 5 CV curves for the $Co_{core}$–$Pt_{shell}$/C before and after accelerated durability testing. The durability test was carried out on the same sample at room temperature in an $O_2$-saturated 0.1-mol/L $HClO_4$ solution at a sweep rate of 10 mV/s

Table 1 Comparison of the Pt/C and $Co_{core}$–$Pt_{shell}$/C

| Sample | ECSA (m² g⁻¹) | $i_{kin}$ (mA cm⁻²) |
|---|---|---|
| Pt/C | 80.1 | 0.199 |
| $Co_{core}$–$Pt_{shell}$/C | 68.1 | 0.386 |

electrochemically active surface areas (ECSA) of the catalysts were calculated to be 68.1 m$^2$/g for Co$_{core}$–Pt$_{shell}$/C nanoparticles and 80.1 m$^2$/g for the BASF Pt catalyst, respectively (Table 1). The lower ECSA value of the Co$_{core}$–Pt$_{shell}$/C nanoparticles can rule out surface roughening as the origin of the enhanced ORR catalytic activity [41]. Actually, the difference in adsorption properties between the supported metal shell and its bulk counterpart has been shown to be a general phenomenon due to the modification of the electronic properties of surface atoms by the underlying metal via geometric strain and ligand interactions. For Pt on a Co surface, compressive strain of the Pt–Pt distance occurs, resulting in weak interactions between the Pt surface atoms and some simple adsorbates such as H, CO, and OH [42, 43]. Furthermore, Co$_{core}$–Pt$_{shell}$ catalyst has the added feature of reduced cost, due to the lower Pt loading.

In order to investigate the electrocatalytic characteristics of the catalysts with regard to the ORR, cathodic reduction from 0.8 V vs. Ag/AgCl in 0.1 M HClO$_4$ solution saturated with oxygen using a rotating disk electrode at 1,600 rpm and a scan rate of 10 mV/s was conducted. As the net kinetic current ($i_{kin}$) is directly proportional to the activity, the $i_{kin}$ values per unit area at 0.6 V allow a comparison of the oxygen reduction activity of the electrocatalysts. Accordingly, the $i_{kin}$ at 0.6 V was obtained according to the formula [44]:

$$i_{kin} = i_{lim} \cdot i_{obs}/(i_{lim} - i_{obs}) \qquad (1)$$

where $i_{lim}$ is the limiting current and $i_{obs}$ is the observed current at 0.6 V. $i_{lim}$ and $i_{obs}$ are elucidated by the example of the cathodic sweep curves shown in Fig. 4. The $i_{kin}$ values listed in Table 1 also allow a comparison of the oxygen reduction activity of the Co$_{core}$–Pt$_{shell}$/C as compared to the BASF Pt electrocatalyst. The $i_{kin}$ value is obviously higher in the Co$_{core}$–Pt$_{shell}$/C electrocatalysts, as shown in Table 1. This result is consistent with the CV results above.

Since the cathode in a fuel cell is exposed to the corrosive environment of the acidic electrolyte and oxygen, the stability of the Co$_{core}$–Pt$_{shell}$/C catalyst must also be studied. So, we performed cyclic voltammetry in O$_2$-saturated 0.1-mol/L HClO$_4$ solutions at a sweep rate of 10 mV/s. After 5,000 cycles, the CV measurements showed a loss of 46% in ECSA for the Co$_{core}$–Pt$_{shell}$/C catalyst (Fig. 5), as compared to 42% for the pure Pt/C catalyst, suggesting that the Co$_{core}$–Pt$_{shell}$ particles had durability similar to that of the pure Pt/C catalyst. At the same time, the current peak in the CV curves obtained after 5,000 cycles is shifted toward anodic potentials and lower. This implies that the activation has a little bit decline.

## Conclusions

Nanosize Co$_{core}$–Pt$_{shell}$ catalysts can be readily fabricated by a successive reduction strategy. The formation of a core–shell structure has been elucidated by various techniques, including XRD, TEM, and electrochemical techniques. The as-prepared catalysts have a uniform distribution, with a particle size in the range of 3–5 nm. Electrochemical testing results indicate that Co$_{core}$–Pt$_{shell}$/C shows an enhanced catalytic activity compared to that of pure Pt/C. Our results show that the Co$_{core}$–Pt$_{shell}$/C nanoparticles could have a promising application in PEM fuel cells as effective catalysts for oxygen reduction, with the added feature of reduced cost.

## References

1. Mallouk TE (1990) Nature 343:515–517
2. Steel BCH, Einzel AH (2001) Nature 414:345–352
3. Perry ML, Fuller TF (2002) J Electrochem Soc 149:559–563
4. Yeager E (1984) Electrochim Acta 29:1527–1532
5. Markovic NM, Schmidt TJ, Stamenkovic V, Ross PN (2001) Fuel Cells 1:105–116
6. Markovic NM, Ross PN (2002) Surf Sci Rep 45:117–229
7. Chen W, Kim J, Sun S, Chen S (2008) J Phys Chem C 112:3891–3898
8. Son SU, Jang Y, Park J, Na HB, Park HM (2004) J Am Chem Soc 126:5026–5027
9. Masatake H, Masakazu D (2001) Appl Catal A 222:427–437
10. Zhang J, Lima FHB, Shao MH, Sasaki K, Wang JX, Hanson J, Adzic RR (2005) J Phys Chem B 109:22701–22704
11. Jun CH, Park YJ, Yeon YR, Choi JR, Lee WR, Ko SJ, Cheon J (2006) Chem Commun 15:1619–1624
12. Galetti A, Gomez M, Arrua L, Abello MC (2008) Appl Catal A 348:94–102
13. Hu JW, Li JF, Ren B, Wu DY, Sun SG, Tian ZQ (2007) J Phys Chem C 111:1105–1112
14. Hu JW, Zhang T, Li JF, Liu Z, Ren B, Sun SG, Tian ZQ, Lian T (2005) Chem Phys Lett 408:354–359
15. Baer R (2004) Nano Lett 4:85–88
16. Park JI, Cheon J (2001) J Am Chem Soc 123:5743–5746
17. Park JI, Kim MG, Jun YM, Lee JS, Cheon J (2004) J Am Chem Soc 126:9072–9078
18. Lee WR, Kim MG, Choi JR, Park J, Ko SJ, Oh SJ, Cheon J (2005) J Am Chem Soc 127:16090–16097
19. Xiang J, Lu W, Hu YJ, Wu Y, Yan H, Lieber CM (2006) Nature 441:489–494
20. Giorgio SS, Penisson JM, Chapon C, Bourgeois S, Henry C (2005) J Phys Chem B 109:342–347
21. Pachon LD, Thathagar MB, Hartl F, Rothenberg G (2006) Phys Chem 8:151–155
22. Takahashi A, Hamakawa N, Nakamura I, Fujitani T (2005) Appl Catal A 294:34–39
23. Rolison DR (2003) Science 299:1698–1701
24. Landsman DA, Luczak FJ (2003) In: Vielstich W, Lamm A, Gasteiger H (eds) Handbook of fuel cells fundamentals, technology and applications, 4th edn. Wiley, Chichester, pp 811–831
25. Mukerjee S, Srinivasan S, Soriaga MP, Mcbreen J (1995) J Electrochem Soc 142:1409
26. Paulus UA, Scherer GG, Wokaun A, Schmidt TJ, Stamenkovic V, Radmilovic V, Markovic NM, Ross PN (2002) J Phys Chem B 106:4181–4191

27. Stamenkovic V, Schmidt TJ, Ross PN, Markovic NM (2002) J Phys Chem B 106:11970–11979
28. Stamenkovic VR, Fowler B, Mun BS, Wang B, Ross PN, Lucas CA, Markovic NM (2007) Science 315:493–497
29. Do JS, Chen YT, Lee MH (2007) J Power Sources 172:623–632
30. Lee MH, Do JS (2009) J Power Sources 188:353–358
31. Kristian N, Wang X (2008) Electrochem Commun 10:12–15
32. Chen YM, Yang F, Dai Y, Wang WQ, Chen SL (2008) J Phys Chem C 112:1645–1649
33. Zhao HB, Li L, Yang J, Zhang YM (2008) Electrochem Commun 10:1527–1529
34. Schmid G, West H, Mehles H, Lehnert A (1997) Inorg Chem 36:891–895
35. Turkevich J, Stevenson PC, Hillier J (1951) Discuss Faraday Soc 11:55–59
36. Askoylu AE, Madalena M, Figueiredo JL (2000) Appl Catal A 192:29–42
37. Wang JX, Markovic NM, Adzic RR (2004) J Phys Chem B 108:4127–4133
38. Stamenkovic VR, Mun BS, Mayrhofer KJJ, Ross PN, Markovic NM (2006) J Am Chem Soc 128:8813–8819
39. Shao MH, Sasaki K, Adzic RR (2006) J Am Chem Soc 128:3526–3527
40. Schmidt TJ, Gasteiger HA, Stab GD, Urban PM, Kolb DM, Behm RJ (1998) J Electrochem Soc 145:2354–2358
41. Wang GX, Wu HM, Wexler D, Liu HK, Savadogo O (2010) J Alloy Compd 503:L1–L4
42. Kitchin JR, Nørskov JK, Barteau MA, Chen JG (2004) Phys Rev Lett 93:156801–156804
43. Greeley J, Mavrikakis M (2004) Nat Mater 3:810–815
44. Tamizhmani G, Dodelet JP, Guay D (1996) J Electrochem Soc 143:18